

## EXPERIMENTAL STUDY OF NUCLEAR FUSION REACTIONS IN A $pt\mu$ SYSTEM

*L. N. Bogdanova*<sup>a</sup>, *D. L. Demin*<sup>b, 1</sup>, *V. N. Duginov*<sup>b</sup>,  
*V. V. Filchenkov*<sup>b</sup>, *K. I. Gritsaj*<sup>b</sup>, *A. D. Konin*<sup>b</sup>,  
*T. N. Mamedov*<sup>b</sup>, *A. I. Rudenko*<sup>b</sup>, *V. A. Stolupin*<sup>b</sup>,  
*Yu. I. Vinogradov*<sup>c</sup>, *V. P. Volnykh*<sup>b</sup>, *A. A. Yukhimchuk*<sup>c</sup>

<sup>a</sup> Institute of Theoretical and Experimental Physics, Moscow

<sup>b</sup> Joint Institute for Nuclear Research, Dubna

<sup>c</sup> Russian Federal Nuclear Center VNIIEF, Sarov, Russia

By means of muon catalysis we study the phenomena in a  $pt$  fusion, which have been previously investigated in the only experiment and now are at the frontier of nuclear few-body physics. The experiment is aimed at measuring the yields of the reaction products:  $\gamma$  quanta, conversion muons and  $e^+e^-$  pairs. As a result, we plan to measure the  $pt$ -fusion partial product yields (first time for  $e^+e^-$  pairs) with accuracy not worse than 10%, and this will enable us to obtain the nuclear reaction rates in M1 and E0 transitions in  $A = 4$  system.

С помощью методов, развитых при решении экспериментальных задач в мюонном катализе, мы изучим явление  $pt$ -синтеза в мюонной молекуле  $pt\mu$ . Это явление исследовалось ранее в единственном эксперименте и находится сейчас в центре внимания ядерной физики многих тел. Эксперимент будет направлен на измерение выходов продуктов реакции синтеза в  $pt\mu$ -молекулах:  $\gamma$ -квантов, конверсионных мюонов и  $e^+e^-$ -пар. В результате мы планируем определить парциальные выходы продуктов  $pt$ -синтеза (впервые для  $e^+e^-$ -пар) с точностью не хуже 10%, что позволит уточнить константы ядерной реакции для M1- и E0-переходов в системе  $A = 4$ .

PACS: 21.45.Ff; 24.70.+s; 25.30.Mr; 25.55.-e

### 1. MUON CATALYZED $pt$ FUSION

**1.1. Background.** At present the processes of muon catalysis (MC) mean the summary of  $\mu$ -atomic and  $\mu$ -molecular processes, caused by a negative muon in hydrogen isotope mixture (H, D, T). This exotic physics is of an independent value and has become a phenomenon of culture. At the same time, MC has numerous important fundamental applications, e.g.:

- 1) muon capture by proton — ST, QCD;
- 2) Lamb shift in  $p\mu$  atom — QED and charge proton radius;
- 3) Precision spectroscopy of a 3-body system — vacuum polarization and relativistic corrections for the weakly bound level in  $dd\mu$  system.

Since 2007, the accurate experimental works on these problems have been carried out at PSI (Switzerland).

---

<sup>1</sup>E-mail: demin@jinr.ru

A notable feature of MC is that it serves as a method for the fusion reaction study under specific conditions: practically zero energy (0.1 keV) of the relative nuclei motion; definite spin and angular momenta for the initial state of the nuclei; absence of electronic screening revealed at low energies.

At present the MC processes have been widely investigated by both theory and experiment. Tens of the experimental works were devoted to the study of  $d + t$  and  $d + d$  cycles, the parameters of the  $p + d$  cycle were measured in about ten experiments and the  $t + t$  cycle was experimentally explored by three experimental groups. As a result, the rates of the muon catalyzed fusion  $d + d$ ,  $p + d$  and  $t + t$  have been measured, and they turned out to be in agreement with the theory.

An extraordinary exception are the results for the  $pt$ -fusion reaction:

$$pt\mu \rightarrow {}^4\text{He} \mu + \gamma + 19.82 \text{ MeV} \quad (E_\gamma = 19.77 \text{ MeV}), \quad (1)$$

$$pt\mu \rightarrow {}^4\text{He} + \mu + 19.81 \text{ MeV} \quad (E_\mu = 19.76 \text{ MeV}), \quad (2)$$

$$pt\mu \rightarrow {}^4\text{He} \mu + e^+ + e^- + 18.79 \text{ MeV} \quad (3)$$

(here we indicate only the dominant reaction channels). These reactions are going from the ground state of the  $pt\mu$  molecule and hence from the  $s$  wave of the initial nuclear system [1]. Since the total  $pt$  spin can be either 1 (initial state  $1^+$ ) or 0 ( $0^+$ ) and the ground state of  ${}^4\text{He}$  is  $0^+$ , the possible transitions are  $1^+ \rightarrow 0^+$  (M1) and  $0^+ \rightarrow 0^+$  (E0).

Experimental study of the reactions (1), (2) was made in the only experiment at PSI [2]. Events of reaction (3) with creation of electron–positron conversion pairs have not been observed by the authors. It appeared that the rate of reaction (1) (M1 transition) exceeds the theoretical value eight times and the rate of the muon conversion (E0 transition) is higher than the theoretically expected value by hundreds of times. It would be desirable to resolve the situation because the study of reactions (1)–(3) is very important for the modern few-body physics.

### 1.2. Importance

1. It is practically impossible to study correctly the  $pt$  fusion from the pure  $s$  wave in the beam–target experiments because even for the smallest energies achievable the appropriate transitions (M1 and E0) are masked by the dominant E1 transition from the  $p$  wave despite the fact that it is suppressed due to the centrifugal barrier. This is illustrated in Table 1 taken from the latest TUNL measurements [3].

Table 1. Strength of different transitions obtained by the authors of [3] from their investigation of the  $pt$  reaction

Collision energy, keV	40	80
E1 strength, %	$99.56 \pm 0.47$	$99.8 \pm 0.7$
M1 strength, %	$0.44 \pm 0.28$	$0.2 \pm 0.06$

2. The theoretical analysis shows that the meson exchange currents (MEC) play a very important role in the radiative  $n + d$  and  $n + {}^3\text{He}$  capture at low energies. The effects which lead to a strong MEC contribution in  $n + d$  thermal neutron capture cross section are expected to be even stronger in the four-body system. In the case of thermal neutron

capture on  ${}^3\text{He}$  the calculated cross section was found to be almost entirely due to exchange currents [4]. Studies were performed for the mirror reactions —  $p + d$  and  $p + t$  capture [3, 5]. The analysis allowed one to conclude that, as in the case of thermal neutron capture on  ${}^3\text{He}$ , the  $s$ -wave cross section in the  ${}^3\text{H}(p, \gamma){}^4\text{He}$  reaction below 80 keV is primarily due to MEC effects. MC reaction (1) can be used for probing of nonnucleonic degrees of freedom in the four-nucleon system and investigating the spin–isospin structure of the MEC operator [6, 7].

3. Since the value of  $S_s$  ( $S$  factor due to the M1 transition) for the  ${}^3\text{H}(p, \gamma){}^4\text{He}$  reaction is closely related to the  ${}^3\text{He}(n, \gamma){}^4\text{He}$  cross section at thermal energies, this result should provide additional tests of the model assumptions and should lead to a more accurate value of the high-energy neutrino flux expected from the  ${}^3\text{He} + p$  reaction in the Sun. The  ${}^3\text{He}(p, e^+\nu)$  reaction is a likely source of high-energy neutrinos in the Sun, where the average proton kinetic energy is of the order of 1 keV. The cross sections are either impossible or very difficult to measure in the laboratory.

4. Electric monopole operator couples the nucleus to muon in the  $pt\mu$ , giving rise to the internal muon conversion process. It also couples the nucleus to the Dirac background to produce electron–positron pairs. The important question is the relation between these two channels. According to MC classics Ya. B. Zeldovich and S. S. Gershtein, the muon conversion rate is  $\sim 10^5 \text{ s}^{-1}$  and the pair-to-muon ratio should be  $R = \mu/e^+, e^- \simeq 0.7$  [8]. According to the current theory [9], based on the relation between the monopole strength determined from the inelastic electron scattering and «traditional» one measured from the internal pair intensities, the nonradiative fusion rate should be significantly smaller than that for radiative fusion in  $pt\mu$ . The pair conversion for the  $pt$  reaction was not observed in flight (beam–target) and in the  $pt\mu$  system. It would be very important to clarify the discrepancy between the theory and the experiment.

**1.3. Analysis of the PSI Experimental Data. Comparison with the  $p+d$  Case.** The results of [2] for the rates  $\lambda_{pt}^f$  of the  $pt$  reaction for the different  $pt$  spin (I) are given in Table 2 together with the appropriate calculations.

Table 2. Experimental [2] and theoretical values for the  $pt$  fusion reactions

Value	Experiment	Theory
$\lambda_{pt}^f(I_{pt} = 1), \mu\text{s}^{-1}$	$0.067^{+0.005}_{-0.002}$	$0.008 \pm 0.0005$ (a) $0.01 \pm 0.003$ (b)
$\lambda_{pt}^\mu(I_{pt} = 0), \mu\text{s}^{-1}$	$0.15 \pm 0.04$	$0.0005 \pm 0.00005$ (c) $\sim 0.1$ (d)
$\lambda_{pt}^{e^+e^-}(I_{pt} = 0), \mu\text{s}^{-1}$	—	$0.0004 \pm 0.00004$ (c)

Theoretical estimations (a, b, c) were obtained using the conventional algorithm [10]:

$$\lambda^f = K^f \cdot G, \quad (4)$$

where  $K^f = \lim_{v \rightarrow 0} (v\sigma^f) C_0^{-2}$  is the reaction constant,  $\sigma^f$  is the reaction cross section,  $C_0^{-2}$  is the Coulomb penetrability (Gamow factor),  $G$  is the probability of nuclear coalescence in the muonic molecule (replaces usual beam flux and target density in the collision experiments). In this case the in-flight data are engaged to calculate the nuclear constant.

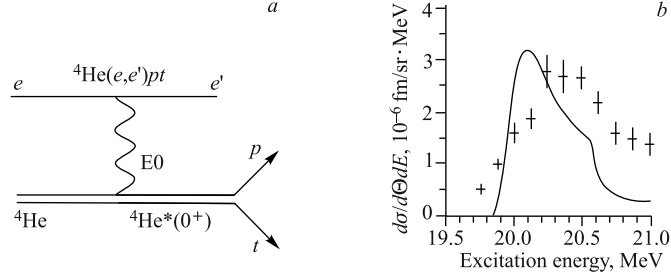


Fig. 1. Diagram for  ${}^4\text{He}(e, e')pt$  process (a) and the appropriate cross section (b)

For estimation of  $\lambda_{pt}^f(I_{pt} = 1)$ , the following data were used:

(a) the cross section of the mirror reaction  ${}^3\text{He}(n, \gamma){}^4\text{He}$  for thermal neutrons:  $\sigma(n, \gamma) = (54 \pm 6) \mu\text{b}$  [9];

(b) the experimental estimation [3] for the M1 strength [9];

(c) these values were obtained with the matrix element for  ${}^4\text{He}$  monopole excitation from  ${}^4\text{He}(e, e')pt$  reaction with taking into account the resonance  ${}^4\text{He}^*$  mechanism [9]. The appropriate diagram is shown in Fig. 1.

Another method: a model calculation without using the experimental nuclear data to estimate  $\lambda_{pt}^\mu(I_{pt} = 0)$  — variant (d) in [11]. Note that the author neglected the above-mentioned resonance.

The sharp contradictions between the measurements and calculations are brightly demonstrated by these data. It is especially surprising if one takes into account the excellent agreement (see Table 3) between the theory and the most accurate measurement of parameters of the  $p + d$  cycle [12] in many features similar to the  $p + t$  one.

Table 3. Experimental [12] and theoretical [13] values for the  $p + d$  fusion reactions

Value	Experiment	Theory
$\lambda_\gamma^f(I_{pd} = 1/2), \mu\text{s}^{-1}$	$0.350 \pm 0.020$	0.39
$\lambda_\gamma^f(I_{pd} = 3/2), \mu\text{s}^{-1}$	$0.110 \pm 0.010$	0.11
$\lambda_\mu^f(I_{pd} = 1/2), \mu\text{s}^{-1}$	$0.056 \pm 0.006$	0.062

The measured and calculated values of the  $pd\mu \rightarrow {}^3\text{He} \mu + \gamma$  fusion rates ( $\lambda_\gamma^f$ ) for different  $pd$  spin ( $I_{pd} = 3/2, 1/2$ ), as well as the rate  $\lambda_\mu^f$  of the nonradiative process  $pd\mu \rightarrow {}^3\text{He} + \mu$ , are given in Table 3. Two different methods were used to analyze the experimental data. Direct *ab initio* calculation of  $\lambda_{pd}^f$  [13] was made by solving the three-body problem using Faddeev equations with realistic nuclear potential. Another analysis [14] was made engaging the data from old bubble chamber experiments. Using the calculations of the spin-averaged value  $\lambda_f^\gamma$  and the value of the  $\gamma$  yield measured in [12], the authors could obtain the  $p + d$  fusion rates close to [13].

## 2. FOUNDATION FOR THE NEW EXPERIMENTAL STUDY OF THE $pt$ CYCLE

In view of the evident discrepancy between the theory and the only experiment [2] on the  $pt$ -cycle parameters and understanding the importance of the experimental results for

intensively developing few-body theory, we intend to perform the experiment on this subject with a new experimental method providing new possibilities for the study.

There are important distinctions between the previous measurement and the one proposed:

1. Not triple H/D/T but double H/T mixture will be used which allows simplifying the data interpretation.

2. Our experiment will be aimed at detecting not only muons and  $\gamma$ 's but  $e^+e^-$  pairs as well. For this aim the special selection criteria will be used including registration of the electron–positron coincidence in time and the analysis of the energy loss in thin detectors surrounding the target.

### 3. KINETICS OF THE PROCESS

The simplified scheme of the processes caused by a negative muon in H/T mixture with a small tritium concentration ( $C_t \sim 1\%$ ) is shown in Fig. 2. Low  $C_t$  should be chosen to avoid the noticeable influence of the  $tt\mu$ -molecule effects, its formation rate  $\lambda_{tt\mu}$  being of the same order as that for  $pt\mu$  molecule ( $\lambda_{pt\mu}/\lambda_{tt\mu} = 2.5$ ).

At each stage of the processes, a muon can decay with the rate

$$\lambda_0 = 0.455 \mu\text{s}^{-1}, \quad (5)$$

which determines the time scale of the kinetics picture.

The liquid H/T mixture will be used in our experiment. So, all  $\mu$ -atomic and  $\mu$ -molecular rates (which are proportional to the mixture density) are given just for the liquid hydrogen density.

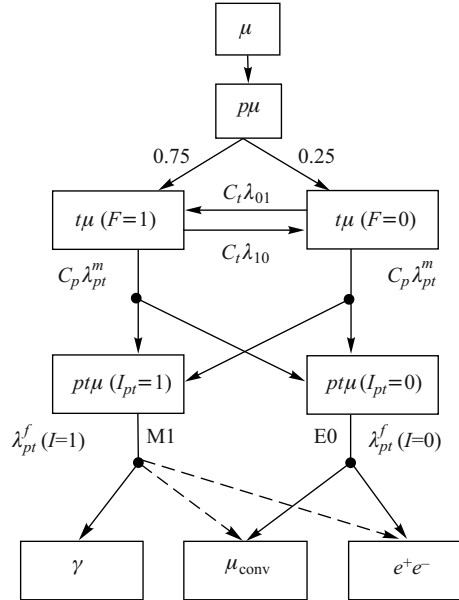
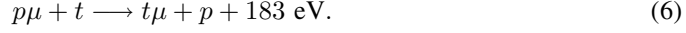


Fig. 2. Simplified scheme of the MC processes in H/T mixture (figure from [2])

The negative muon stopped in the hydrogen forms predominately  $p\mu$  atom, then it is quickly transferred to tritium forming  $t\mu$  atom:



The measured transfer (6) rate is  $\lambda_p = (9.3 \pm 1.5) \cdot 10^3 \mu\text{s}^{-1}$  [2], which is somewhat higher than predictions of theory [15].

So, in our experimental conditions the «effective» transfer rate would be  $\lambda'_p = \lambda_p \cdot C_t = 100 \mu\text{s}^{-1}$ , that is the process takes only tens of nanoseconds. Note that  $\lambda'_p$  is much higher than the rate of the competing process of the  $pp\mu$ -molecule formation ( $\lambda_{pp\mu} \simeq 3 \mu\text{s}^{-1}$ ).

In collisions of  $t\mu$  atom with hydrogen molecules, the  $pt\mu$  molecule can be formed:



The rate of the  $pt\mu$  formation, measured in [2], is  $\lambda_{pt\mu} = (7.5 \pm 1.3) \mu\text{s}^{-1}$ . Being initially formed in the excited state,  $pt\mu$  molecule de-excites rapidly ( $10^{-12}$  s) via Auger transition to the ground state  $(J, \nu) = (0, 0)$  ( $J, \nu$  are the rotational and vibration quantum numbers), where the dominant configuration of  $p-t$  relative motion is  $L = 0$  [1]. Thus, almost pure  $s$  state of the  $pt$  system is selected, both spin configurations  $I_{pt} = 1, 0$  being possible.

The  $pt\mu$  ground state is split into three hyperfine structure (h.f.s.) substates with the total angular momenta  $j = 3/2, 1/2, 1/2^*$  [16] (see Fig. 3). As is seen from the figure, the  $pt$  configurations with total spin  $I_{pt}$  have different weights ( $W$ ) for the  $pt\mu$  h.f.s. states: state with  $j = 3/2$  corresponds only to  $I_{pt} = 1$ , and both  $I_{pt} = 1, 0$  can populate the other states.

A remarkable feature is that the population of the h.f.s. states of  $pt\mu$  depends on the  $t\mu$ -atom spin state  $F$ : for  $F = 1$  all three h.f.s. states of  $pt\mu$  can be occupied and only two states with  $j = 1/2, 1/2^*$  can be populated for  $F = 0$  (see Table 4). It means that the fusion reaction yields must depend on the  $t\mu$ -atom spin. This «Gershtein–Wolfenstein effect» was predicted in 1961 [17] for the  $p+d$  cycle and then confirmed in several experiments, most accurately in [12].

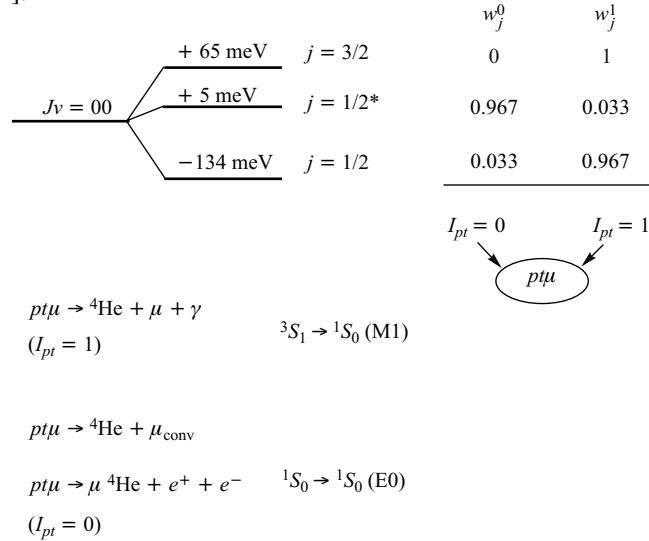
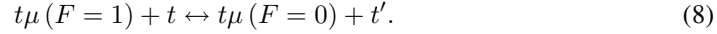


Fig. 3. Hyperfine structure of  $pt\mu$  ground state (figure from [7])

Table 4. Population of the  $pt\mu$  h.f.s. levels for different  $t\mu$ -atom spin states  $w_j$  [16]

$t\mu$ -atom spin state	$j = 3/2$	$j = 1/2^*$	$j = 1/2$
$F = 1$	0.6667	0.2960	0.0373
$F = 0$	0	0.8880	0.1120
Statistical mixture $F = 1, F = 0$	0.5000	0.2500	0.2500

The atom  $t\mu$  is initially formed in the statistical mixture of its spin states:  $3/4$  with  $F = 1$  and  $1/4$  for  $F = 0$ . In collisions with tritium atoms the spin-flip processes can occur:



The measured value for the process (8) rate is  $\lambda_{10} = (1 \pm 0.2) \cdot 10^3 \mu\text{s}^{-1}$  [2] which is in an accordance with the most recent calculations ( $1.3 \cdot 10^3 \mu\text{s}^{-1}$ ) [18].

In the transfer process (6),  $t\mu$  atom acquires the kinetic energy  $E_{t\mu}^0 \simeq 46$  eV and then decelerates in collisions with atoms (molecules) of the mixture. Process (8) remains reversible until  $t\mu$  kinetic energy  $E_{t\mu}$  exceeds the energy of the  $t\mu$ -atom hyperfine splitting  $\Delta E_{\text{hp}} = 0.282$  eV; that is, the statistical mixture of the  $t\mu$ -atom spin states is conserved. The problem is that the deceleration process is rather slow because it proceeds mainly in the collisions of  $t\mu$  atoms with tritium of relatively low concentration ( $C_t \simeq 0.01$ ). As to the  $t\mu + p \rightarrow t\mu + p$  collisions, their cross section has a deep Ramsauer minimum at  $E_{t\mu} \sim 1$  eV [19]. The results of [2] indicate that the  $t\mu$ -atom deceleration time is  $\simeq 100$  ns. It means that for low tritium concentration  $C_t \leq 0.001$ , the statistical mixture of  $F = 1, 0$  would dominate in  $pt\mu$  formation. Contrary, for higher  $C_t \geq 0.02$ , the  $t\mu$  spin state with  $F = 0$  would give the main input to this process.

## 4. EXPERIMENT

**4.1. Choice of the Experimental Conditions.** As we noted, the liquid H/T mixture will be used. The tritium concentration in it is limited by the relations:

- 1)  $\lambda_p \cdot C_t \gg (\lambda_{pp\mu} + \lambda_0)$ , which corresponds to  $C_t \geq 0.005$ ,
- 2)  $\lambda_{pt\mu} \gg (\lambda_{tt\mu} \cdot C_t + \lambda_0)$ , which corresponds to  $C_t \leq 0.02$ .

Based on these «boundary conditions», we choose the tritium concentration  $C_t = 0.01$ .

**4.2. Experimental Method.** The experimental method is based on the measurements of the reaction product yields (1)–(3) with appropriate delayed time coincidence scheme for registering the experimental events and the analysis of the amplitude and time distributions in the corresponding experimental spectra.

*4.2.1. Installation.* The schematic view of the experimental layout is shown in Fig. 4.

*4.2.2. Target.* For the proposed experiment we will construct a liquid tritium target with a general design close to the one described in [20] and used by us in the recent study of  $tt$ -fusion reaction [21]. The new target will have the enlarged ampoule volume — 50 cc. It will contain H/T liquid mixture (1% T, 99% H) at temperature 22 K. The target cylinder-shaped ampoule will be made of stainless steel. The gas-supply system will be the same as in our previous experiments with D/T mixtures [22].

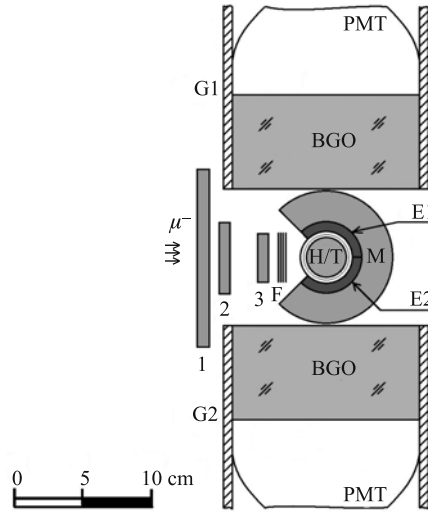


Fig. 4. The proposed installation: 1–3 — muon telescope plastic counters; BGO — scintillation crystals; E1, E2 — electron plastic counters; F — copper degrader; G1, G2 — gamma detectors; H/T — target; M — muon plastic counter; PMT — photomultiplier

4.2.3. *Detection System.* The detection system will be analogous to that described in [23]. A set of scintillation counters (1–3 in Fig.4) are used to detect muon stops in the target volume. To detect electrons from  $\mu$  decay, conversion muons and pairs from  $pt$ -fusion reactions, the detectors (E1, E2) and muon detector M of spectroscopic quality are used. The cylinder plastic scintillator detectors E1, E2 of thickness 5 mm are surrounded with the cylinder plastic scintillator detector M of thickness 20 mm. The heights of the detectors are about 100 mm.

The results of GEANT-4 Monte Carlo simulation of the energy deposited in detectors E1, E2 relative to conversion muons and pairs are shown in Fig.5. The energy and angular distributions of electron–positron pairs (typical for E0 transition) were taken from the work [24] for this simulation.

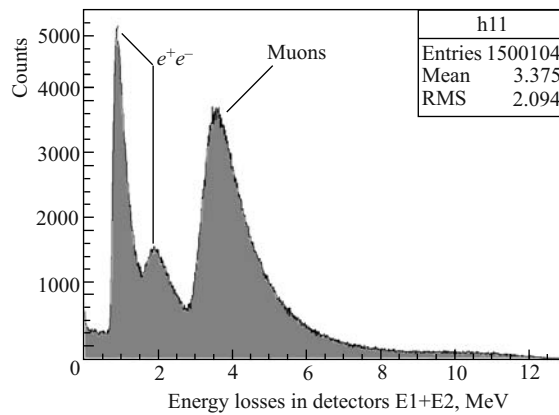


Fig. 5. The simulated sum ( $\mu$  and  $e^+e^-$ ) energy spectrum in detectors E1 + E2

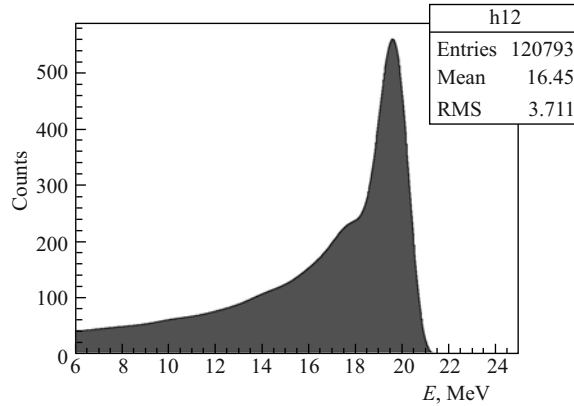


Fig. 6. The simulation of 19.8 MeV  $\gamma$  energy spectrum inside BGO crystal

The minimum thickness of the detector M (20 mm) was chosen to provide the full stop of the conversion muon passing through this detector. It follows from our calculations that 66% (solid angle) of all conversion muons will stop inside the M detector depositing the energy up to 10–12 MeV with the mean value of 8–9 MeV.

Two large identical  $\gamma$  detectors G1, G2 (see Fig. 4) provide the high efficiency for detection of 19.8 MeV  $\gamma$  quanta from the studied reaction. The detectors are made on the base of two BGO crystals supplied by IIC SB RAS (Novosibirsk) [25], each of diameter 127 mm and height 60 mm. The detector study (registration efficiency, energy resolution, energy calibration) was made at VNIIEF (Sarov, Russia), see [26].

The GEANT-4 Monte Carlo simulation of the energy spectrum of 19.8 MeV  $\gamma$  quanta in the detector G is shown in Fig. 6.

We also demand the detection of a decay electron manifesting the disappearance of a muon stopped in the target. «Decay electrons 1» from decay of muons stopped in the target are registered by the detectors E1, E2, M. Decay electron 1 would appear after gamma and pair production in the target. The GEANT-4 simulation of the decay electron 1 registration efficiency gives the value  $\epsilon(e_{d1}) = 70\%$ .

In case of a conversion muon (stopped in counter M) in the output channel of the reaction, its decay electron will be registered with the detectors M, G1, G2 (decay electron 2). The GEANT-4 simulation of the decay electron 2 registration efficiency gives the value  $\epsilon(e_{d2}) = 30\%$ .

Involving of the  $\mu$ -decay electron in the trigger allows the sharp discrimination of the background connected with the muon stops in the target walls.

**4.2.4. Electronics.** The simplified scheme of the electronics is shown in Fig. 7. The coincidence signal  $1 \cdot 2 \cdot 3 \cdot \bar{E}1 \cdot \bar{E}2$  starts the timing gate with the duration of 20  $\mu$ s when the  $\gamma$ -particle or conversion muon (or electron–positron pair) signals are permitted to be registered. The necessary condition for it is an absence of the other incoming muon, detected as coincidence signal  $1 \cdot 2$ , during preceding 5  $\mu$ s. The signal from the Mu-stop block starts the Gate block, producing the digital timing gate. In the same block the electron selection is realized, via the coincidence signal  $(E1 + E2) \cdot M$ . The Trigger block selects the useful events. It monitors signals from detectors and produces the signal permitting the writing of the analogue signals from detectors E1, E2, M, G1, G2. The trigger system is based on Field

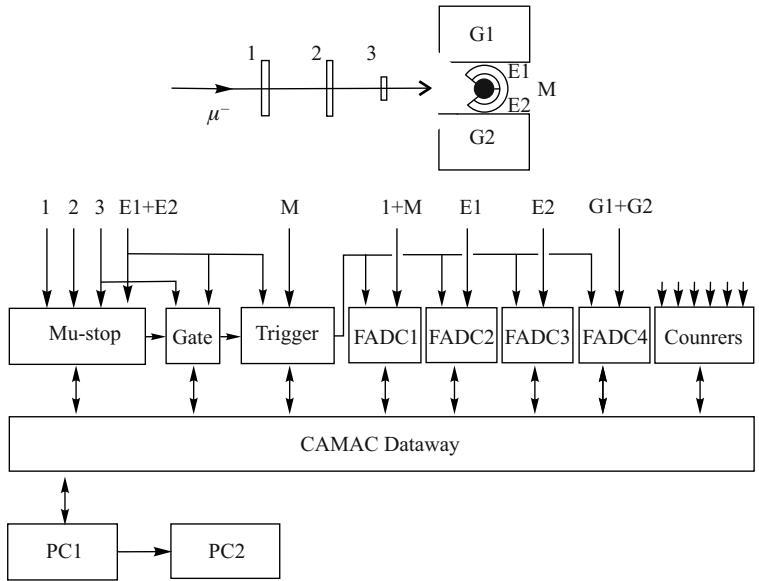


Fig. 7. Block diagram of the electronics

Programmable Gate Array Integrated Circuit [27]; the logic part of the trigger is analogous to that of [28].

The detector signals come to the flashes ADC and are recorded to the personal computer PC1 if they satisfy the delay coincidence  $(\mu, e)$  during the gate. The on-line handling of data is made on the PC2.

4.2.5. *Experimental Conditions.* The properties of the negative muon beam of the JINR Phasotron can be found in Table 5 (see also [29]).

Table 5. Parameters of the required muon beam

Momentum, MeV/c	$100 \pm 5\%$
Beam spot FWHM, cm <sup>2</sup>	4 · 4
Intensity, s <sup>-1</sup>	$3 \cdot 10^3$

For the liquid H/T target exposed to the negative muon beam, the muon stop rate would be  $100 \text{ s}^{-1}$ . The data taking will consume 100 h of beam time.

**4.3. Selection of Events.** By the «experimental event» we imply the aggregate of the appropriate detectors signals caused by muons stopped in the target. They are selected according to the usual MC experiments scheme of the delayed coincidences

$$\mu_s \text{ --- } x \text{ --- } e_d$$

Here  $\mu_s$  is the marker of the muon stopped in the target. It is formed as a signal combination 1-3,  $\bar{E}1, \bar{E}2$ . Marker  $e_d$  corresponds to the electron from muon decay inside the target. It is the logical sum  $e_d = e_{d1} + e_{d2}$ , where:

- $e_{d1}$  is the coincidence signal  $(E1 + E2) \cdot M$ , responsible for the muon stop in the target;
- $e_{d2} = (\bar{E}1 + \bar{E}2) \cdot M \cdot (G1 + G2)$  means conversion muon decay in detector M.

Marker  $x$  notes the fusion reaction products:  $\gamma$ ,  $e^-e^+$  or conversion muon. The appropriate signals are the following:

- $x = \gamma$ :  $(\bar{E}1 + \bar{E}2) \cdot \bar{M} \cdot G$ , the decay electron selected as  $e_{d1}$ ;
- $x = \mu$ : the coincidence signal  $(E1 + E2) \cdot M$ , and  $e_{d2}$  for the electron from muon decay;
- $x = e^-e^+$ :  $(E1 + E2) \cdot M$ , and  $e_{d1}$  corresponds to detection of at least one particle of the pair;
- $E1 \cdot E2 \cdot M$ , and the subsequent  $e_{d1}$  corresponds to simultaneous detection of both particles of the pair with their coincidence in time.

For a more reliable identification of the registered experimental events and the background suppression, one should put certain timing limitations, usual in MC experiments:

$$\text{a) } t(e_{d1}) - t(\mu) > 0.5 \mu\text{s}, \quad \text{b) } t(e_{d1}, 2) = t_x + (0.5-4.5) \mu\text{s}. \quad (9)$$

The condition a) is necessary to reject the background (mainly X rays) caused by the muon stop in the target wall. The condition b) is introduced to separate the fusion product from the decay electron and limits its time interval to decrease its own background. The criteria (9) lead to some additional loss in the detection efficiency with the factor

$$f_t \simeq 40\%. \quad (10)$$

The time (relative to the muon stop) and the energy losses for the selected events registered in the detectors E1, E2, M, G1, G2 will be accumulated in the appropriate histograms and used in the further analysis.

## 5. THE DATA ANALYSIS

The measured yields of the  $pt$ -reaction products and their time distributions will be analyzed. We accept, in the first approximation, that the  $pt$  spin state  $I_{pt} = 1$  is accompanied predominately with gamma production, and  $I_{pt} = 0$  state results in muon and pair production. So, we have the expression for the time distribution of the fusion reaction products typical for two studied processes ( $pt\mu$  formation and then fusion in it):

$$\frac{dN_y}{dt} = A_y \frac{\lambda_{pt\mu} \lambda_y^f}{\lambda_{pt\mu} - \lambda_y^f} [\exp(\lambda_0 + \lambda_y^f) - \exp(\lambda_0 + \lambda_{pt\mu})]. \quad (11)$$

Here  $y$  denotes fusion rate for  $\gamma$  quanta, muons and pairs. The value of the normalization coefficient  $A_y$  depends on the  $t\mu$ -atom spin state (see Fig. 3 and Table 4).

Integration of (11) leads to a simple factorization

$$Y_y = A_y f_1 f_2, \quad (12)$$

where  $f_1 = \lambda_{pt\mu}/(\lambda_{pt\mu} + \lambda_0)$  is the probability of the  $pt\mu$  formation,  $f_2 = \lambda_y^f/(\lambda_y^f + \lambda_0)$  is the probability of the fusion in channel  $y$ .

The estimations for the absolute yields  $Y^0(y)$  for all types of fusion products are given in Table 6.

Table 6. Estimations for the absolute yields  $Y^0(y)$  of  $pt$ -reaction products for different  $t\mu$ -atom spin states

Fusion products	Statistical mixture $F = 1.0$			$F = 0$		
	Muons	Gammas	Pairs	Muons	Gammas	Pairs
Experiment [2]	0.062	0.0960	—	0.028	0.114	—
Theory [9]	0.000275	0.0127	0.000575	0.00012	0.015	0.00056

Experimental yields will be, of course, essentially smaller (by an order of magnitude) due to the finite efficiency of the reaction products and decay electrons detection. The number of detected  $\mu$ -decay electrons will be used for normalization

$$N_\mu = \frac{N^{\text{det}}(e_{d1})}{\epsilon(e_{d1})} + \frac{N^{\text{det}}(e_{d2})}{\epsilon(e_{d2})}, \quad (13)$$

where  $N_\mu$  is the number of muons stopped in the target,  $N^{\text{det}}(e_d)$  and  $\epsilon(e_d)$  are the number of detected electrons and their detection efficiency.

Fitting the experimental time distributions for  $\gamma$ 's, muons and pairs, we determine  $\lambda_{pt\mu}$  from the «fast» slope and  $\lambda_y^f$  from the «slow» slope of the time spectra. Identification of the fusion product type will be made according to the «strong» criteria, described in Subsec. 5.3. Comparison of the fusion rates extracted from the time distributions for muons and electrons allows estimation of the possible yield of pairs from the states with  $I_{pt} = 1$ .

**5.1. Measured Number of Events. Statistical Accuracy.** The measurements will be carried out on the muon beam of JINR Phasotron providing the intensity of muon stops in the target  $\simeq 100 \text{ s}^{-1}$ . It means that for 100 h of the accelerator operation we could accumulate the total muon number

$$N_\mu \simeq 4 \cdot 10^7.$$

The number of detected events for each sort ( $y$ ) of the fusion products is

$$N_y = N_\mu Y^0(y) \text{eff}(y),$$

where  $Y^0(y)$  is the absolute yield and  $\text{eff}(y)$  are the detection efficiencies:

$$\begin{aligned} \text{eff}(\gamma) &= \epsilon(\gamma)\epsilon(e_{d1})f_t, & \text{eff}(\mu) &= \epsilon(\mu)\epsilon(e_{d2})f_t, \\ \text{eff}(\text{pairs } 1) &= \epsilon(\text{pairs } 1)\epsilon(e_{d1})f_t, & \text{eff}(\text{pairs } 2) &= \epsilon(\text{pairs } 2)\epsilon(e_{d1})f_t. \end{aligned}$$

The registration efficiencies  $\epsilon(y)$ ,  $\epsilon(e_d)$  were calculated by the GEANT-4 package. They are presented in Table 7.

If one takes the values of  $Y^0(y)$  from Table 6 founded on the PSI results,  $\epsilon(y)$ ,  $\epsilon(e_d)$  from Table 7 and  $f_t$  according to (10), then one obtains the values of the measured yield  $Y^{\text{det}}(y)$  and numbers of detected events which are presented in Table 8. For the estimations we put the pair yield to be equal to the muon one.

As is seen from Table 8, we provide the statistics reserve enough for the reliable determination of the relative yields for all fusion products of the  $pt$  reaction. This statistics allows determination of the partial fusion rates from the slope of «slow» exponent in the corresponding time distribution (11).

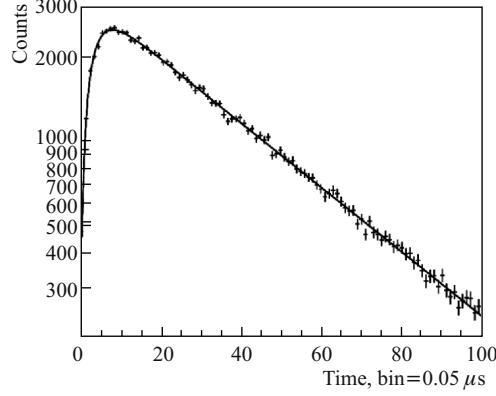


Fig. 8. The  $\gamma$  time spectrum, simulated according to expression (9) with the initial values  $\lambda_{pt\mu} = 6.5 \mu\text{s}^{-1}$  and  $\lambda_{pt}^f = 0.067 \mu\text{s}^{-1}$ . Line reflects the fit result

Table 7. Simulated efficiencies

Particles	Registration efficiency, %
$\epsilon(\gamma)$	20
$\epsilon(\mu)$	66
$\epsilon(\text{pairs } 1)$	90
$\epsilon(\text{pairs } 2)$	16
$\epsilon(e_{d1})$	70
$\epsilon(e_{d2})$	30

To estimate the possible statistical errors in the exponent slopes (fusion rates), we simulated (Monte Carlo) the  $\gamma$  time distribution with the initial values  $\lambda_{pt\mu} = 6.5 \mu\text{s}^{-1}$  and  $\lambda_{pt}^f = 0.067 \mu\text{s}^{-1}$ . The simulated spectrum is presented in Fig. 8. Its total statistics is  $N_\gamma \simeq 1.1 \cdot 10^5$ . The parameters found from the fit are shown in Table 9. As one can see, there is an excellent agreement between initial values and those obtained from the fit. Note that uncertainty in the slope of the «slow» component is  $\Delta = 0.003/0.528 = 0.57\%$ . The statistical error estimated from the total statistics  $\Delta_0 = \sqrt{1/N_\gamma} = 0.3\%$ , that is, 1.8 times smaller. This comparison gives us a possibility to estimate the accuracy in  $\lambda_{pt}^f$  for the obtained statistics.

So, it follows from the data presented in Table 8 that the absolute statistical error in  $\lambda_{pt}^f$  is expected to be  $\Delta(\lambda_{pt}^f) \simeq 0.002 \mu\text{s}^{-1}$  (for example,  $\lambda_{pt}^{f;\gamma} = (0.070 \pm 0.002) \mu\text{s}^{-1}$ ). If the appropriate yield will turn out to be smaller ( $k$  times), the relative accuracy will change for the worse radically:  $k\sqrt{k}$  times. If  $k = 10$ , then our example becomes  $\lambda_{pt}^{f;\gamma} = (0.007 \pm 0.006) \mu\text{s}^{-1}$ .

Table 8. Estimations for statistics of the  $pt$ -fusion products (for the statistical mixture of the  $t\mu$ -atom states)

Reaction product	Absolute yield $Y^0(y)$	Detection efficiency $\text{eff}(y)$	Measured yield $Y^{\text{det}}(y)$	Number of events $N^{\text{det}}(y)$
Gammas	0.096	0.056	0.0054	$\simeq 2.2 \cdot 10^5$
Muons	0.062	0.079	0.0049	$\simeq 2.0 \cdot 10^5$

Better statistical accuracy can be obtained using the yields of the fusion products. So even for  $k = 100$  the fusion rate is 100 times smaller than the one measured in [2], the statistical accuracy would be at the level of few percent. Of course, in this case we encounter the uncertainty connected with not well defined  $t\mu$ -atom spin state. As it follows from the data

Table 9. Results of the analysis of simulated  $\gamma$  time distribution (in  $\mu\text{s}^{-1}$ )

Fit procedure	$\lambda_{pt\mu}$	«Fast» slope $\lambda_{pt\mu} + \lambda_0$	$\lambda_{pt}^{f,\gamma}$	«Slow» slope $\lambda_{pt}^{f,\gamma} + \lambda_0$
Initial values	6.5	6.955	0.067	0.522
Fit results	$6.59 \pm 0.19$	$7.04 \pm 0.19$	$0.073 \pm 0.003$	$0.528 \pm 0.003$

shown in Table 7, the gamma yield differs for the different spin states by a factor of 1.2, and the muon one by 2.2. These factors will define the limits for values of the corresponding partial fusion rates.

**5.2. Background Subtraction.** *5.2.1. Gamma Background.* As it follows from our experimental investigations of the rare reaction  $dd\mu \rightarrow {}^4\text{He} + \gamma + \mu + 24.8 \text{ MeV}$  [23], the total (accidental and connected with the muon beam) background will be not more than  $10^{-6}/\mu$  for the energy threshold of 15 MeV. It is three orders less than the estimated  $\gamma$  yield, which is  $4 \cdot 10^{-3}$ .

*5.2.2. Charged Particle Background.* The source of the background for muons and pairs is the accidental counts for E1, M and E2, M coincidences, which are mainly caused by the cosmic radiation. Their level may be estimated from our previous experiments with similar geometry:  $3 \cdot 10^{-5}/2 \mu\text{s}$ , that is 0.5% relative to the muon yield measured at PSI. If the yields of muons and (or) pairs will be smaller by two orders, then the relative background will be at the level of the effect. The analysis of the appropriate time and energy loss ( $E$ ) distributions will be used for the effective background-effect separation.

**5.3. Systematic Uncertainties.** *5.3.1. Detection Efficiency.* The detection efficiency of both the fusion products  $\epsilon(y)$  and of  $\mu$ -decay electrons  $\epsilon(e_d)$  were calculated with package GEANT-4 for the suggested geometry of the experiment. The dominant uncertainty is due to poorly known space distribution of the muon stops in the target, and its value does not exceed  $\delta(\epsilon)/\epsilon = 5\%$ .

*5.3.2. Identification of the Fusion Products.* As we noted, the criterion for  $\gamma$ 's is the absence of a signal from detectors (E1, E2). However, there is a small probability to detect  $\gamma$ 's by these detectors mainly due to Compton interaction and the detection of pairs from the  $\gamma$  conversion on the target wall. According to our consideration, this probability is  $w(\gamma - e) = (3 \pm 1)\%$ . For  $\gamma$ 's it means only insignificant loss in the detection efficiency. It is more serious that it leads to false pairs (the same criterion for the  $\mu$ -decay electron is used for  $\gamma$ 's and pairs) and distorts both their time distribution and yield. The necessary corrections will depend on the relative pair yield: the more is the gamma/pair ratio, the more this correction is. The appropriate uncertainty can achieve tens of percent. Fortunately, we have the very reliable way to determine the pair yield measuring the electron-positron coincidences which will be known with an accuracy of  $\simeq 5\%$  (from  $\epsilon(e^-e^+)$ ). So, the appropriate corrections can be made.

*5.3.3. Uncertainties in Normalization.* The necessary requirement for the trigger is the detection of the  $\mu$ -decay electron. The electrons are registered in all cases including the «empty» registration gate (without signals from the fusion) and are used for normalization. There exists a possibility to accept as a  $\mu$ -decay electron a signal from (E1, E2) detector caused by a pair (even single particle:  $e^-$  or  $e^+$ ) or conversion muon. So, the correction for these false electrons should be made. Obviously, the value of this correction depends strongly

on the muon or pair yield. Common expression for the relative corrections  $\delta_e$  is

$$\delta_e = \frac{N_e^{\text{false}}}{N_e^{\text{real}}} = Y_y^{\text{det}} \frac{(1 - \epsilon(e_d))}{\epsilon(e_d)}. \quad (14)$$

Based on the data of Table 8, we put for a maximum estimation  $Y_y^{\text{det}} \simeq 1\%$ . Then we obtain for pairs

$$\delta_e(\text{pairs}) \simeq 0.01 \cdot (1 - 0.7)/0.7 \simeq 0.5\%, \quad \delta_e(\text{muons}) \simeq 0.01 \cdot (1 - 0.3)/0.3 \simeq 2\%.$$

As is seen, both corrections are small and can be easily accounted from the measured muon and pair yields.

*5.3.4. Electron Time Spectra.* The determination of the number of electrons originating from muon decay will be done in the analysis of the electron time spectra obtained in the experiment. For the exposures with H/T filled target we will fit the electron time spectra using the expression

$$N_e^{\text{tot}}(t) = A_e \exp(-\lambda_e t) + k B_{\text{empty}}(t) + F,$$

where  $\lambda_e$  is the muon disappearance rate;  $B_{\text{empty}}(t)$  is the time-dependent background induced by muons stopped in target walls;  $F$  is the accidental background. In this fit  $k$ ,  $A_e$ ,  $\lambda_e$ , and  $F$  are parameters. The fitting of the electron time spectra from muons stopped and decayed in the walls of the empty target will allow us to obtain the shape of the electron background distribution  $B_{\text{empty}}(t)$ .

As a result, we will receive the number of electrons  $N_e = A_e/\lambda_e$  from the muons stopped in hydrogen mixture. The  $N_e$  is necessary for the normalization.

## CONCLUSION

If the measured yields of the  $pt$ -fusion products turn out to be of the same order as they were measured in the previous experiment [2], then we shall be able to determine the corresponding fusion rates with an accuracy not worse than 10%. (Only  $\gamma$ 's and muons were detected in [2], but we expect that the pair yield would be approximately the same as the muon one.) If the yield for some fusion products appears lower by an order of magnitude, then the error will be significantly larger (tens of percent).

However, we have an additional source of information, namely, the values of the partial yields. Even if the muon and (or) pair yields appear to be hundred times smaller than ones measured in [2] (according to the «standard» theory), we shall be able to determine their relative yield with an accuracy of 5–7%. Analysis of these values with an attraction of known data on the  $t\mu$ -atom deceleration process will allow us to obtain more definite information for the  $pt$  partial fusion rates.

In any case we will measure the  $pt$ -fusion product yields (first time for pairs) with an accuracy not worse than 10%. A confirmation of the discrepancy between theory and experiment concerning the value of the monopole matrix element would be the only example when monopole strength for excitation of  $0^+$  states extracted from  $(e, e')$  measurements differ from those obtained with traditional methods (observation of pairs or conversion electrons/muons) [30].

It would very interesting to extract the nuclear matrix elements in the  $A = 4$  system by means of *ab initio* calculations in modern theory. Now such a theory is intensively developed. By now a series of works have already been performed, for instance [31–33]. The work [31] («*Ab Initio* Four-Body Calculations of  $n-^3\text{He}$ ,  $p-^3\text{H}$ ,  $d-d$  Scattering») is of special importance for us because it includes the consideration of the  $p + t$  interaction. It would be very interesting to make *ab initio* calculations just for E0 transition. In this case one could compare the theoretical nuclear constant with the one extracted from the muon catalysis experimental data that would be a sensitive test for the theory.

#### REFERENCES

1. *Vinitskii S. I., Melezhik V. S., Ponomarev L. I.* // Sov. J. Nucl. Phys. 1982. V. 36. P. 272.
2. *Baumann P. et al.* // Phys. Rev. Lett. 1993. V. 70. P. 3720;  
*Hartmann F. J. et al.* // Hyp. Int. 1993. V. 82. P. 259.
3. *Canon R. S. et al.* // Phys. Rev. C. 2002. V. 65. P. 044008.
4. *Wervelman R. et al.* // Nucl. Phys. A. 1991. V. 526. P. 265.
5. *Rice B. J. et al.* // Phys. Rev. C. 1997. V. 56. P. R2918.
6. *Bogdanova L. N., Markushin V. E.* // Intern. Workshop on Pions in Nuclei, Penyscola, Spain, June 2–9, 1991 / Eds. E. Oset, M. Vicente-Vacas, C. Garcia-Recio. World Sci. Publ., 1991. P. 570.
7. *Markushin V. E., Baumann P., Hartmann F. J.* // Hyp. Int. 1993. V. 77. P. 161.
8. *Zeldovich Ya. B., Gershtein S. S.* // Usp. Fiz. Nauk. 1960. V. LXXI. P. 619; Sov. Phys. Uspekhi. 1961. V. 3. P. 593.
9. *Bogdanova L. N., Markushin V. E.* // Nucl. Phys. A. 1990. V. 508. P. 29c;  
*Bogdanova L. N., Filchenkov V. V.* // Hyp. Int. 2001. V. 138. P. 321.
10. *Jackson J. D.* // Phys. Rev. 1957. V. 106. P. 330.
11. *Zubarev A. L.* // Phys. Lett. B. 1992. V. 295. P. 187.
12. *Petitjean C.* // Hyp. Int. 2001. V. 138. P. 191.
13. *Friar J. L. et al.* // Phys. Rev. Lett. 1991. V. 66. P. 1827.
14. *Bogdanova L. N., Markushin V. E.* // MCF. 1990/1991. V. 5/6. P. 189.
15. *Matveenko A. V., Ponomarev L. I.* // Zh. Eksp. Teor. Fiz. 1970. V. 58. P. 1640; Sov. Phys. JETP. 1970. V. 31. P. 880;  
*Melezhik V. S.* // MCF. 1987. V. 1. P. 205.
16. *Bakalov D. D., Vinitskii S. I., Melezhik V. S.* // Zh. Eksp. Teor. Fiz. 1980. V. 79. P. 1629; Sov. Phys. JETP. 1980. V. 52. P. 820.
17. *Gershtein S. S.* // Zh. Eksp. Teor. Fiz. 1961. V. 40. P. 698; Sov. Phys. JETP. 1961. V. 13. P. 488.
18. *Bracci L. et al.* // Phys. Lett. A. 1989. V. 134. P. 435.
19. *Bubak M., Faifman M.* JINR Commun. E4-87-464. Dubna, 1987.
20. *Yukhimchuk A. A. et al.* // Fusion Science and Technology. 2005. V. 48. P. 294.
21. *Bogdanova L. N. et al.* // Zh. Eksp. Teor. Fiz. 2009. V. 135. P. 242; JETP. 2009. V. 108. P. 216.
22. *Yukhimchuk A. A. et al.* // Hyp. Int. 1999. V. 119. P. 341;  
*Bom V. R. et al.* // Zh. Eksp. Teor. Fiz. 2005. V. 127. P. 752; JETP. 2005. V. 100. P. 663.
23. *Baluev V. V. et al.* // JETP. 2011. V. 113. P. 68.
24. *Montoya C. P. et al.* // Nucl. Instr. Meth. A. 1993. V. 334. P. 437.
25. *Gusev V. A. et al.* // Nucl. Instr. Meth. A. 2001. V. 460. P. 457.

26. *Generalov L. N. et al.* VNIIEF Preprint 104-2009. Sarov, 2009.
27. *Zinov V. G., Rudenko A. I., Sidorov V. T.* JINR Preprint P13-96-439. Dubna, 1996.
28. *Dzhelepov V. P. et al.* // *Zh. Eksp. Teor. Fiz.* 1992. V. 101. P. 1105; *Sov. Phys. JETP.* 1992. V. 74. P. 589.
29. *Demianov A. V. et al.* JINR Commun. P9-93-374. Dubna, 1993.
30. *Kibedi T., Spear R. H.* // *At. Data and Nucl. Data Tables.* 2005. V. 89. P. 77.
31. *Deltuva A., Fonseca A. C.* // *Phys. Rev. C.* 2007. V. 76. P. 021001(R).
32. *Deltuva A., Fonseca A. C., Sauer P. U.* // *Phys. Lett. B.* 2008. V. 660. P. 471.
33. *Deltuva A., Fonseca A. C.* // *Phys. Rev. C.* 2010. V. 81. P. 054002;  
*Viviani M., Deltuva A., Lazauskas R.* arXiv: 1109.3625v1. 2011.

Received on April 2, 2012.